Structural and transport properties in the Ag_3SI system: a molecular dynamics study of alpha, beta and molten phases

2004 J. Phys.: Condens. Matter 16 181

(http://iopscience.iop.org/0953-8984/16/3/001)

INSTITUTE OF PHYSICS PUBLISHING JOURNAL OF PHYSICS: CONDENSED MATTER

J. Phys.: Condens. Matter **16** (2004) 181–194 PII: S0953-8984(04)69716-5

Structural and transport properties in the Ag_3SI system: a molecular dynamics study of alpha, beta and molten phases

S Matsunaga[1] **and P A Madden**[2]

[1] Division of General Education, Nagaoka National College of Technology, Nagaoka 940-8532, Japan
[2] Physical and Theoretical Chemistry Laboratory, Oxford University, South Parks Road, Oxford OX1 3QZ, UK

Received 1 October 2003
Published 9 January 2004
Online at stacks.iop.org/JPhysCM/16/181 (DOI: 10.1088/0953-8984/16/3/001)

Abstract

Structural properties of the β phase and transport properties of the superionic (α), β and molten phases of Ag_3SI are investigated by molecular dynamics simulation (MD), using Vashishta–Rahman (VR)-type potentials. In the β phase, the pair distribution functions are quite different from those in the α phase, because anions form the order arrangement in a bcc structure in the β phase, whereas anions occupy the lattice points randomly in the α phase. The silver distributions obtained in the β phase are in good agreement with experimental results, which are quite different from those in the α phase, as we reported in a previous paper. The conductivities obtained in the α and β phases by MD are also in good agreement with experiments. The frequency dependent diffusion coefficients in the α and β phases, which are derived from the temporal Fourier transformation of the velocity autocorrelation function, have similar features to the neutron TOF spectra data.

1. Introduction

Superionic conductors are a group of substances which exhibit high values of ionic conductivity whilst in the solid state [1]. They have been of considerable interest because of their technological importance and their novel physical behaviour. Silver sulfide iodide is one of the superionic conductors of the group AgI, Ag_2S and Ag_3SI, which is the most widely studied. Among them, the compound Ag_3SI was first reported in 1965 by Reuter and Hardel [2–4]. At temperatures above 519 K, Ag_3SI shows its superionic phase, i.e. α-phase, with a bcc structure of disordered arrangement of anions, S and I ions.

In a previous paper [5] (hereafter referred to as paper I), we used a set of Vashishta–Rahman (VR)-type pair potentials [6, 7] to obtain the pair distribution functions $g_{ij}(r)$ and other structural properties for Ag_3SI in the α and molten phases by molecular dynamics simulation

Table 1. The values of parameters in the potential sets used in the MD simulations.

The particle radii (Å)	$\sigma_{\mathrm{I}} = \sigma_{\mathrm{S}} = 2.11$
	$\sigma_{\mathrm{Ag}} = 0.69$
The effective valence (e)	$Z_{\mathrm{Ag}} = 0.6$
	$Z_{\mathrm{I}} = -0.6$
	$Z_{\mathrm{S}} = -1.2$
The repulsive strength (e^2 Å^{-1})	
For Ag–Ag, Ag–I, I–I, I–S	$A_1 = 0.0123$
For Ag–S, S–S	$A_2 = 0.0150$
The electronic polarizability (e^2 Å^{-1})	$\alpha_{\mathrm{Ag}} = 0$
	$\alpha_{\mathrm{I}} = 6.52$
	$\alpha_{\mathrm{S}} = 6.52$

(MD). The structural properties by MD in the α phase are in good agreement with recent experimental work [8]. These MD results have shown that these potential sets are capable of reproducing the main features of the static structure of this system.

As a continuation of our work, we report the results of the structural properties in the β phase and transport properties in the β, α and molten phases of the Ag_3SI system. After we submitted paper I, we discovered the earlier MD work on Ag_3SI by Ihara and Suzuki [9]. Our structural results in the α phase are similar to their results. They have also obtained the structural properties in the β phase and the transport and dynamical features in the α and β phases, though their potentials do not include a term for the charge–dipole interactions. And it seems that the discussions of the temperature dependence of the results may not be sufficient. These facts prompt us to investigate the structural properties in the β phase and the transport and dynamical features in the β, α and molten phases by MD using VR-type potentials.

2. Method

The MD method, that we used in this study, is essentially similar to that used in paper I. We briefly summarize as follows. We used VR-type potentials [6, 7] for MD simulations. These are written as follows.

$$V_{ij}(r) = A_{ij}\left(\frac{\sigma_i + \sigma_j}{r}\right)^n + \frac{Z_i Z_j e^2}{r} - \frac{1}{2}(\alpha_i Z_j^2 + \alpha_j Z_i^2)\frac{e^2}{r^4} \tag{2.1}$$

where i, j stand for the type of ions. The first term models the overlap repulsion between the ions, where A_{ij} is the repulsive strength, and σ_i, σ_j are the particle radii. The second is the Coulomb interaction between the effective charge. Z_i, Z_j are the effective valence, which we choose so as to preserve the condition of electric neutrality. e stands for the elementary charge. The third term is the effective charge–dipole interaction, where the α_i are the electronic polarizabilities. The values of $\sigma_{\mathrm{I}}, \sigma_{\mathrm{S}}$ and σ_{Ag} are determined from the lattice structure of the γ phase of Ag_3SI as: $\sigma_i + \sigma_j =$ nearest neighbour distance. For the repulsive interaction value for S–I, we use $A_1\{(\sigma_{\mathrm{I}} + \sigma'_{\mathrm{S}})/r\}^7$ where $\sigma'_{\mathrm{S}} = (A_2/A_1)^7 \times \sigma_{\mathrm{S}}$ [10]. The values of the parameters used are listed in table 1.

The MD calculations were carried out for 1080 (648Ag + 216S + 216I) atoms in a cubic cell. The values of the lattice constant L in the α phase are taken from the experimental data of Didisheim *et al* [11]. Periodic boundary conditions are used, and the long-range Coulomb interaction is handled by the Ewald method. The particles are allocated to the initial position of the crystal structure of the γ phase, and initial velocities with a Maxwellian distribution at

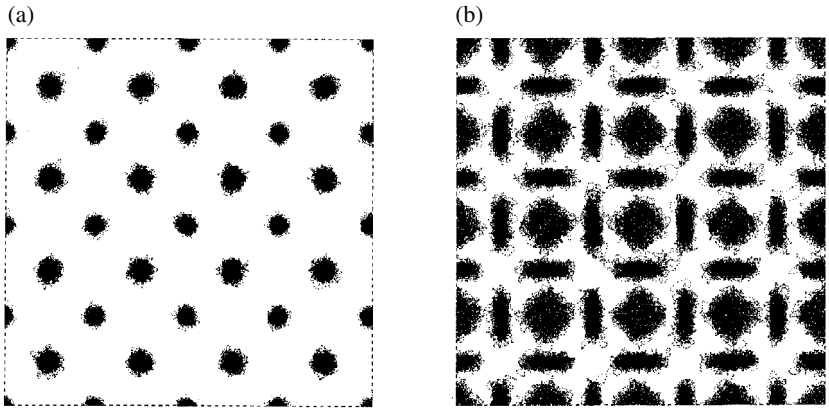

Figure 1. Trajectories of (a) anions and (b) cations at 450 K, projected onto a face of the cube.

a specified temperature, which is kept constant using the Nose method [12] in the constant volume. One time step $\Delta t = 2.0 \times 10^{-15}$ s is used in Verlet's [13] integration algorithm.

3. The structure in the β phase

As reported in paper I, we have investigated the structural features of Ag_3SI in the α phase. In order to compare with them, we calculate the ionic distributions in the β phase, the temperature region for which is between 157 K and 519 K [14]. In our simulation, we first place the atoms on the positions of the γ phase. Then we increase the temperature to the arbitrary point of the β phase, and then, the system is equilibrated for 3000 time steps at that temperature. For the calculations of the average quantities of interest, 5000–30 000 time steps are performed.

3.1. The density distribution of cations

The positions of the ions in a lattice of the β phase have been investigated by several authors [3, 8, 11, 15, 16]. In the β phase, I and S anions exhibit an ordered arrangement in a bcc structure, such as that of Cs and Cl ions in a CsCl lattice, with I located in position $(0, 0, 0)$ and S in $(1/2, 1/2, 1/2)$. Three Ag ions are distributed statistically at the 12(h) site in the unit cell, $(x, 1/2, 0)$, with the x-parameter changing with temperature.

Figures 1(a) and (b) show typical examples of trajectories in β phase at 450 K by MD, which are obtained by the positions of the ions at each period of $20\Delta t$ over the interval of $30\,000\Delta t$ with dots. The trajectories of 128 anions (a) and 192 cations (b) are projected onto the basal plane. It is clearly seen that the anion sublattice is stable and of bcc structure. On the other hand, the Ag ions spread on the $(1, 0, 0)$ plane in the β phase. As we described in paper I, the Ag ions in the α phase make diffusive motion alone 'band' distribution, which is very different from the present result.

As is seen in figure 1(b), the Ag ions are gathered around the centre of the $(1, 0, 0)$ plane. In figures 2(a) and (b), we show the density distribution of the Ag ions by drawing grid (a) and contour lines (b) on a $(1, 0, 0)$ plane of thickness $L/10$, L being the lattice constant. As is clearly seen from the contour lines of Ag ion densities in figure 2(b), they are preferentially distributed in the vicinity of the 12(h) sites, whose positions are described as $(x, 1/2, 0)$. At 450 K, the x-parameter obtained by MD is 0.39, which is very close to the experimental value of 0.407 at 436 K [11].

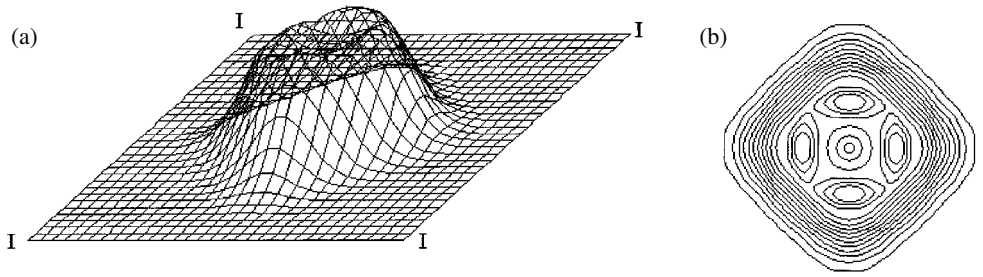

Figure 2. The density distribution of Ag ions by drawing (a) grid and (b) contour lines on a (1, 0, 0) plane at 450 K. Iodine ions at the lattice points are marked I.

As mentioned in section 1, Ihara and Suzuki [9] have performed the MD simulation in the α and β phases using potentials which do not include a term for the charge–dipole interactions. Their structural results for the β phase showed that the Ag ions were localized at the 6(b) site, which is obviously different from our results that the Ag ions reside in the vicinity of the 12(h) site. Such fine structure that appears in our result seems to come from a difference of the potentials used, i.e. the effect of the polarization term in the potential sets. This fact may show that it is necessary to include a polarization term to perform a detailed structural analysis.

3.2. Pair distribution functions

The pair distribution functions for this ternary system are defined as follows.

$$\langle n_{\alpha\beta}(r)\rangle \Delta r = 4\pi r^2 \Delta r \rho_\beta g_{\alpha\beta}(r), \tag{3.1}$$

where $n_{\alpha\beta}(r)\Delta r$ denotes the number of β-type particles around an α-type particle between spherical shells of radii r and $r + \Delta r$. The bracket $\langle\,\rangle$ denotes the thermal average as well as the average over all α-type particles, and ρ_β is the mean number density of the β-type particles [17].

Figures 3(a) and (b) show the partial pair distribution functions for S–S, I–I, S–I, Ag–S, Ag–I, and Ag–Ag at 485 K. As is shown in figure 3(a), the peaks in $g_{SS}(r)$, $g_{SI}(r)$ and $g_{II}(r)$ are sharp like those of a crystal in a thermal agitation. From the first and second peaks of $g_{SS}(r)$ and $g_{II}(r)$, the first and second nearest neighbour separation between S–S, and I–I are found to be 4.8 and 6.8 Å, respectively. Their coordination number (area under the first peak, i.e., up to the first arrow) is 6. The next nearest neighbour coordination (i.e., the second arrow) is found to be 18 (6 + 12). From the first and second peaks of $g_{SI}(r)$, the first and second nearest neighbour separation between S–I is found to be 4.1 and 8.0 Å, respectively. Their coordination number is 8. The next nearest neighbour coordination is estimated to be 32 (8 + 24). These coordination numbers indicate that the anions form an ordered arrangement in a bcc lattice, in which half of the lattice points are occupied by S ions and the rest by I ions.

From figure 3(b), the first peak in $g_{AgS}(r)$ is narrow and appears at 2.45 Å. Its coordination number is 6. On the other hand, the first peak in $g_{AgI}(r)$ is broad and appears at 2.7 Å. The distance of the first neighbour separation between Ag and I is rather closer than that is expected from I on a lattice point and Ag on a 12(h) site. This fact may be explained by the large thermal vibration of I ions from their lattice points, as seen in figure 2. The coordination number of $g_{AgI}(r)$ is 12. The $g_{AgAg}(r)$ has a significant shoulder around 4.0 Å and broad peaks at 5.0 and 6.8 Å corresponding to the localized distribution of Ag ions. As we reported in paper I, these features are very different from $g_{AgAg}(r)$ in the α phase, which shows a similar distribution

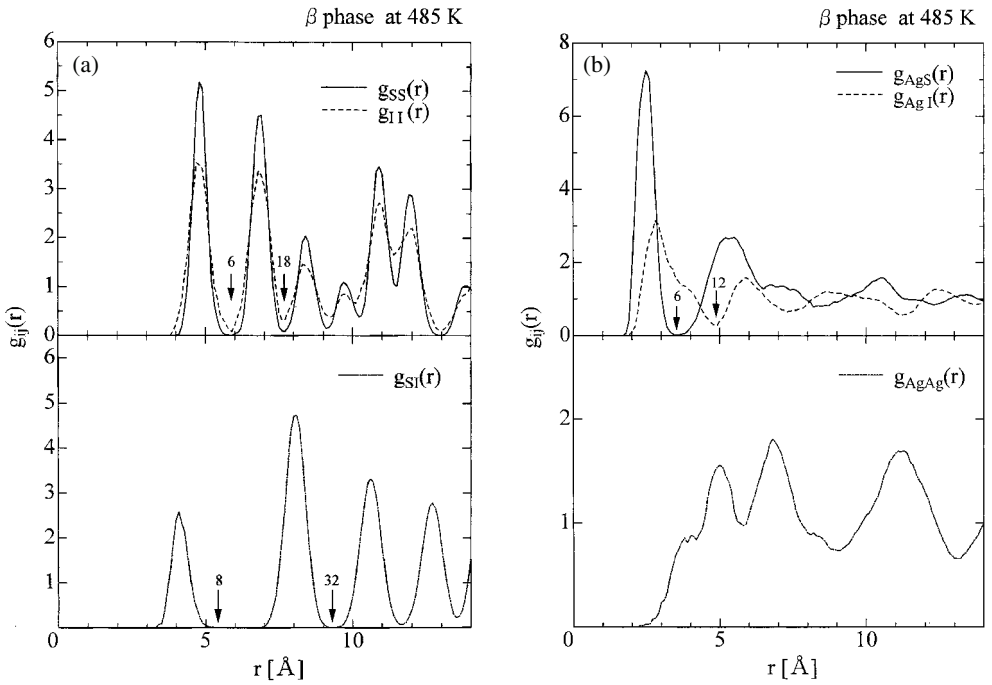

Figure 3. The partial pair distribution functions for S–S, I–I, S–I (a), and Ag–S, Ag–I, and Ag–Ag (b) at 485 K.

as in the liquid state. These characteristic features of partial pair distribution functions are consistent with the distributions of ions seen in figure 2.

4. Transport properties

We now examine the transport properties in the molten, α and β phases. In paper I, we reported the diffusion coefficients obtained by MD in the α and molten phases. In this section, first we calculate the conductivities and other quantities. Next, we discuss the frequency dependent diffusion coefficient in relation to the experimental data.

4.1. Electric conductivities and other quantities

The method of calculation of electric conductivities is essentially similar to that used in previous work [18, 19]. Electric conductivities in the α and molten phases of Ag_3SI at several temperatures are calculated by nonequilibrium MD (NEMD), which is performed in the presence of the external field $\boldsymbol{E}$. The procedure is carried out over 20 000 time steps. The stationary electric current $\boldsymbol{j}$ is, in due course, induced through the increase of net velocities in the direction of $\boldsymbol{E}$, and converges after sufficient time steps on

$$\boldsymbol{j} = \sum_{i=1}^{N} z_i \boldsymbol{v}_i \tag{4.1}$$

where z_i and $\boldsymbol{v}_i$ are the effective charge and the velocity of particle i, respectively. The relation between electric current and electric field is indicated as follows:

$$e\boldsymbol{j} = \sigma V \boldsymbol{E} \tag{4.2}$$

where σ is the electric conductivity, V is the volume of the MD cell, and e is the elementary charge. The electric conductivity σ represents a sum of the partial conductivities, $\sigma = \sigma_{Ag^+} + \sigma_{S^{2-}} + \sigma_{I^-}$. When the external field is varied, the electric current is varied in proportion to the electric conductivity. Therefore, the electric conductivity is derived from this gradient. In NEMD, the partial conductivities are obtained from the following relations:

$$\begin{aligned} e\boldsymbol{j} &= e\boldsymbol{j}_{\mathbf{Ag^+}} + e\boldsymbol{j}_{\mathbf{S^{2-}}} + e\boldsymbol{j}_{\mathbf{I^-}} \\ &= \sigma_{Ag^+} V \boldsymbol{E} + \sigma_{S^{2-}} V \boldsymbol{E} + \sigma_{I^-} V \boldsymbol{E}. \end{aligned} \tag{4.3}$$

Electric conductivities in the β phase of Ag_3SI at several temperatures are calculated by equilibrium MD (EMD). The procedure is carried out over 5000 time steps. The electric-current correlation functions are averaged from 3000 samples in the following method [18, 19]. The electric-current correlation function $J(t)$ without any external field is defined as

$$J(t) = \langle \boldsymbol{j}(t)\boldsymbol{j}(0) \rangle, \tag{4.4}$$

with

$$\boldsymbol{j}(t) = \sum_{i=1}^{N} z_i \boldsymbol{v}_i(t) \qquad \text{and} \qquad \langle \boldsymbol{j}(t) \rangle = \mathbf{0} \tag{4.5}$$

where N is the total number of ions, and $\boldsymbol{v}_i(t)$ is the velocity of the particle i at time t. The total current $\boldsymbol{j}(t)$ can be written as

$$\boldsymbol{j}(t) = \boldsymbol{j}^+(t) + \boldsymbol{j}^-(t) \tag{4.6}$$

where $\boldsymbol{j}^+(t)$ and $\boldsymbol{j}^-(t)$ stand for the electric current for cations and anions, respectively.

In the β phase of Ag_3SI, the electric current is caused by cations. Therefore, the partial conductivity for cations, which is the 'total' conductivity in the β phase, is given by integrating the projection $\boldsymbol{j}(0)$ onto $\boldsymbol{j}^+(t)$, $\langle \boldsymbol{j}^+(t)\boldsymbol{j}(0) \rangle$ as

$$\sigma^+ = \frac{e^2}{3k_B T V} \int_0^\infty \langle \boldsymbol{j}^+(t)\boldsymbol{j}(0) \rangle \, \mathrm{d}t \tag{4.7}$$

where k_B is the Boltzmann constant, and T the absolute temperature.

The results of electric conductivities obtained in the α and molten phases are shown in figure 4. Agreement between the experimental data and MD results is very good in the α phase. As is seen in figure 4, the total conductivity decreases on melting. A similar phenomenon of conductivity decreasing on melting is known in AgI [20]. Ohno *et al* [21] estimated the total ionic conductivity of molten Ag_3SI at 1123 K experimentally, though they have not obtained the temperature dependence of the total ionic conductivity and their result is about twice as large as the MD result. We believe that our results of conductivity are not far from reality, because the collective motion between cations in the α phase, which may enhance the ionic conductivity in the α phase, are thought to be abating in molten phase.

In the molten phase, it may be noteworthy that the total conductivities and partial conductivities increase linearly with the rise in temperature. Furthermore, it seems that the conductivities and partial conductivities have a constant ratio to each other in spite of increasing temperature. The averages of the ratio of the partial conductivities, σ_S/σ_I and σ_{Ag}/σ_I are 1.73 ± 0.07 and 1.43 ± 0.01, respectively. In the molten binary system, it is known that the ratio of the partial conductivities is in inverse proportion to their mass ratio [22]. The present results of conductivities in the molten phase may suggest that a similar relation also may hold

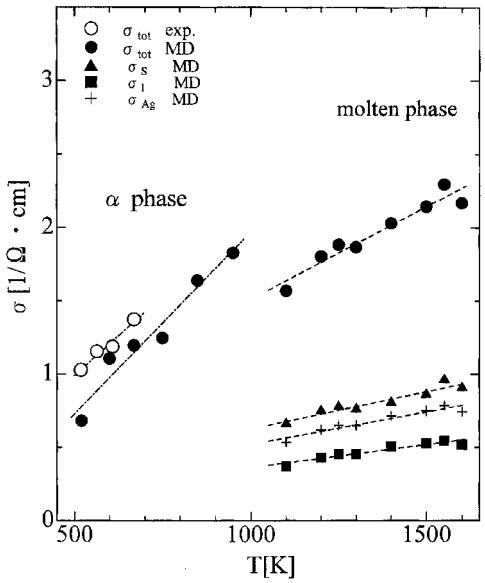

Figure 4. The total and partial electric conductivities in the α and molten phases compared with experimental data.

Table 2. The relation of the partial conductivities at various temperatures.

T (K)	1200	1300	1500
$m_S \cdot \sigma_S/\|Z_S\| + m_I \cdot \sigma_I/\|Z_I\|$	0.965	1.168	1.351 ($\times 10^4$ kg Ω^{-1} m^{-1} mol^{-1})
$m_{Ag} \cdot \sigma_{Ag}/\|Z_{Ag}\|$	0.965	1.168	1.351 ($\times 10^4$ kg Ω^{-1} m^{-1} mol^{-1})

true in molten ternary ionic systems. In fact, as is seen in table 2, the partial conductivities obtained satisfy the following result:

$$m_S \cdot \sigma_S/|Z_S| + m_I \cdot \sigma_I/|Z_I| = m_{Ag} \cdot \sigma_{Ag}/|Z_{Ag}|, \tag{4.8}$$

where m_i is the mass of ion i. This equation is equivalent to the relation of the conservation of the total momentum of ions [23].

Figure 5 shows the current–current correlation functions at various temperatures in the β phase. Their convergence is adequate for time, though the difference of oscillation depending on temperature can be seen in figure 5. The conductivities obtained by MD are shown in figure 6 together with experimental data [24]. Their agreement is very good.

Next, we obtain the deviation from the Nernst–Einstein relation in the molten phase. The partial conductivities are related to the partial diffusion coefficients as

$$\sigma_{Ag^+} = \frac{n_{Ag^+} Z_{Ag^+}^2 e^2}{k_B T} D_{Ag^+}(\mathbf{1} - \Delta_{Ag^+}), \tag{4.9}$$

$$\sigma_{S^{2-}} = \frac{n_{S^{2-}} Z_{S^{2-}}^2 e^2}{k_B T} D_{S^{2-}}(1 - \Delta_{S^{2-}}), \tag{4.10}$$

$$\sigma_{I^-} = \frac{n_{I^-} Z_{I^-}^2 e^2}{k_B T} D_{I^-}(\mathbf{1} - \Delta_{I^-}), \tag{4.11}$$

and the total conductivity is expressed as

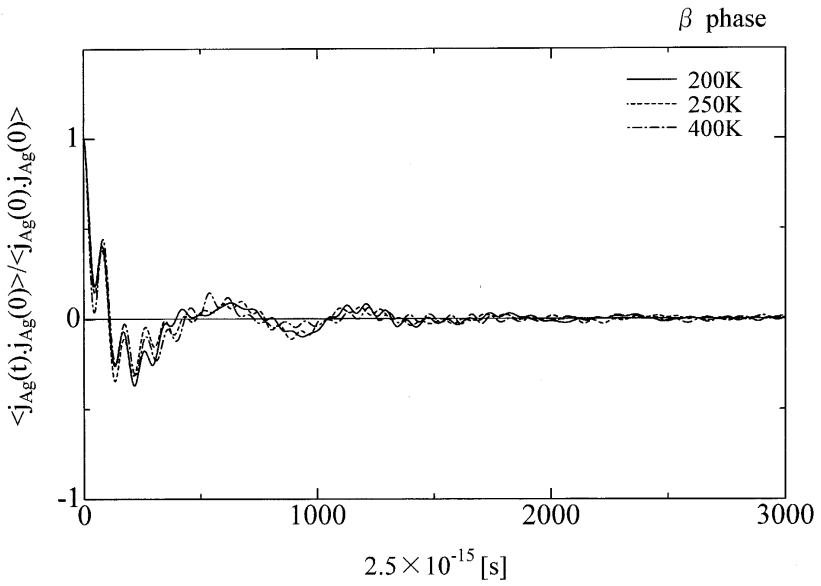

Figure 5. The current–current correlation functions at various temperature in the β phase.

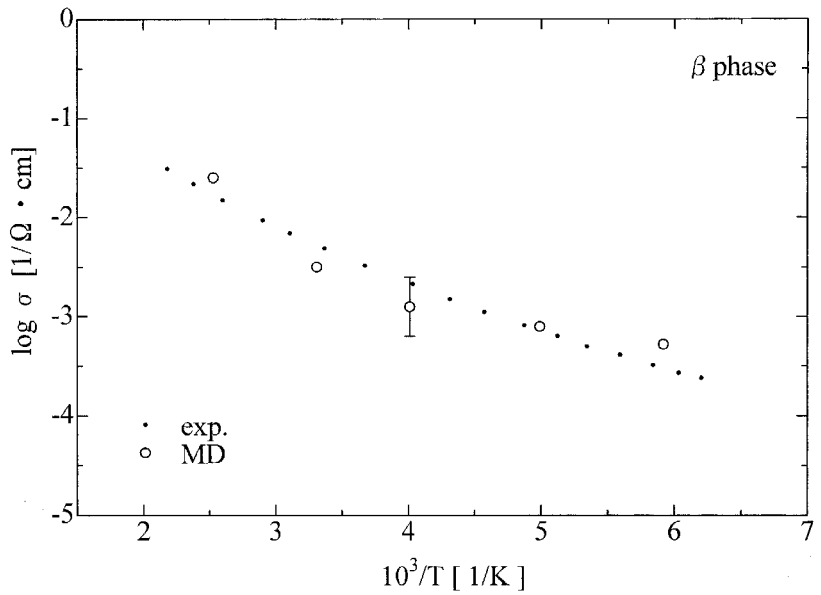

Figure 6. The conductivities obtained by MD in the β phase compared with experimental data.

$$\sigma_{\mathrm{tot}} = \sigma_{\mathrm{Ag^+}} + \sigma_{\mathrm{S^{2-}}} + \sigma_{\mathrm{I^-}}$$
$$= \frac{e^2}{k_{\mathrm{B}}T}(n_{\mathrm{Ag^+}} Z^2_{\mathrm{Ag^+}} D_{\mathrm{Ag^+}} + n_{\mathrm{S^{2-}}} Z^2_{\mathrm{S^{2-}}} D_{\mathrm{S^{2-}}} + n_{\mathrm{I^-}} Z^2_{\mathrm{I^-}} D_{\mathrm{I^-}})(\mathbf{1} - \Delta) \qquad (4.12)$$

where Z_i is the effective valence, D_i is the diffusion coefficient, n_i is the number density, and Δ_i and Δ are deviations from the Nernst–Einstein relation for the conductivity of ion i and for

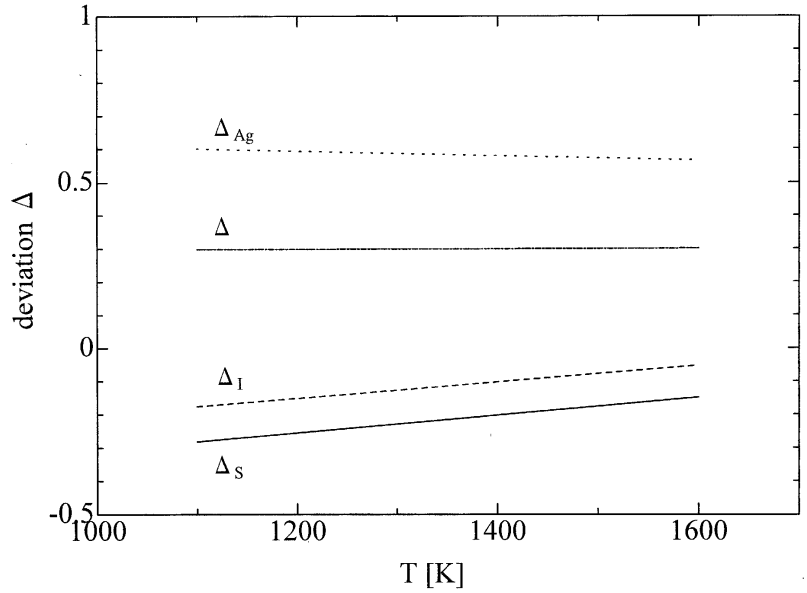

Figure 7. Deviation from the Nernst–Einstein relation for the conductivities of ions, Δ_{Ag^+}, $\Delta_{S^{2-}}$, Δ_{I^-} and for the total conductivity Δ.

the total conductivity, respectively. Δ and Δ_i are related in the following equation as

$$\Delta = \frac{n_{Ag^+} Z_{Ag^+}^2 D_{Ag^+} \Delta_{Ag^+} + n_{S^{2-}} Z_{S^{2-}}^2 D_{S^{2-}} \Delta_{S^{2-}} + n_{I^-} Z_{I^-}^2 D_{I^-} \Delta_{I^-}}{n_{Ag^+} Z_{Ag^+}^2 D_{Ag^+} + n_{S^{2-}} Z_{S^{2-}}^2 D_{S^{2-}} + n_{I^-} Z_{I^-}^2 D_{I^-}}. \tag{4.13}$$

As is seen in figure 7, Δ_{Ag^+} are positive, whereas $\Delta_{S^{2-}}$, and Δ_{I^-} are negative. This fact may suggest that anions move collectively in the molten state because of the large repulsive force acting between them. A 'caterpillar'-like mechanism has been proposed by Yokota [25] to explain the collective motion in the transport properties of superionic conductors. A similar mechanism may exist in the molten phase of this system. The different signs of Δ_i between anions and cations have been observed in molten AgI [26]. As is seen in figure 7, the deviations $\Delta_{S^{2-}}$ and Δ_{I^-} approach zero as the temperature increases, which may suggest that collective motion in molten state abates.

The friction constant γ_i for i-type ions is defined by the Langevin equation [27]. The relation between the friction constant and electrical conductivity for i-type ions σ_i, is written as

$$\sigma_i = \frac{n_i Z_i^2 e^2}{m_i \gamma_i}. \tag{4.14}$$

Therefore, the friction constants are directly derived from the partial conductivities using the above relation. As is seen in figure 8, the friction constants decrease as a function of temperature. Since the friction constants represent the magnitude of the interference of motion, this temperature dependence is consistent with the increasing of the conductivities and diffusion coefficients as the temperature increases. It is also interesting that the friction constant γ_{I^-} is smaller than γ_{Ag^+} at any temperature. This result may be caused by the effect that the attractive force acting on Ag^+ from a neighbouring S^{2-} ion brings about a larger friction constant for the Ag^+ ion. This surmise may ensured by the fact that the first peak of $g_{AgS}(r)$ is seen in the closest position among the partial pair distribution functions in the molten state [5].

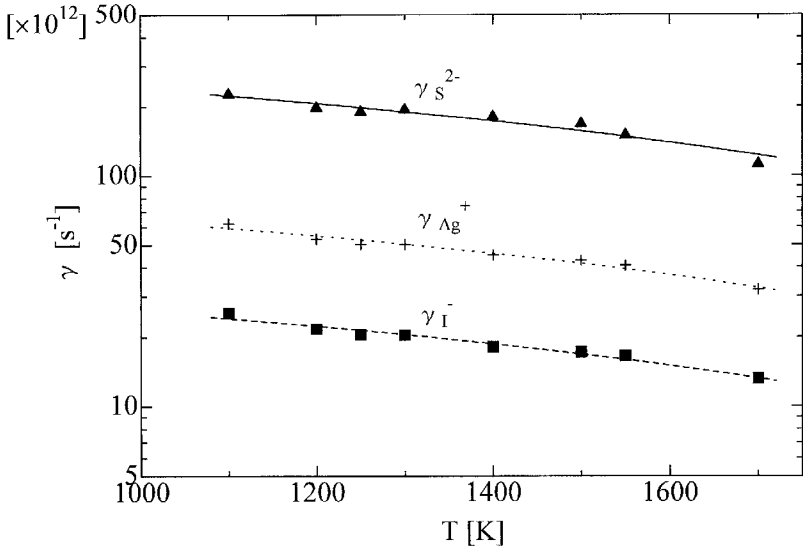

Figure 8. The temperature dependence of friction constants for Ag^+, S^{2-} and I^-.

4.2. Velocity autocorrelation functions and frequency dependent diffusion coefficients

So far, we have studied the electric conductivities and other quantities related to them. Finally, we obtain the velocity autocorrelation function (VAF) to explain the dynamical behaviour of this system. The VAF for ξ-type ions is defined as [17],

$$\Phi_i(t) = \frac{\sum_{i(\xi)} \langle v_i(t) \cdot v_i(\mathbf{0}) \rangle_\xi}{\sum_{i(\xi)} \langle v_i(\mathbf{0}) \cdot v_i(\mathbf{0}) \rangle_\xi}, \tag{4.15}$$

where $v_i(t)$ is the velocity of the ith ion at time t.

The obtained VAFs in the molten, α and β phases are shown in figure 9. The amplitude of the VAF of Ag^+, S^{2-} and I^- decreases with increasing temperature. In particular, the amplitude of S^{2-} is the largest in all phases. In general, the motion of particles is oscillatory when the amplitude of the VAF of the particles is large. Therefore, it is known that the probability of S^{2-}, which has an oscillating motion, decreases with increasing temperature.

Next, we obtain the frequency dependent diffusion coefficients in the molten, α and β phases to compare with neutron time-of-flight (TOF) spectra data. The Fourier transformation of $\Phi_\xi(t)$ is given by [28]

$$\Phi_\xi(\omega) = \int_0^\infty \mathrm{d}t\, \Phi_\xi(t) \mathrm{e}^{\mathrm{i}\omega t}. \tag{4.16}$$

The frequency dependent diffusion coefficient $D_\xi(\omega)$ is obtained from $\Phi_\xi(\omega)$:

$$D_\xi(\omega) = \frac{k_\mathrm{B}T}{m_\xi} \Phi_\xi(\omega). \tag{4.17}$$

The static limit value of $\Phi_\xi(\omega)$ is related to the self-diffusion coefficient, D_ξ, as

$$D_\xi = \frac{k_\mathrm{B}T}{m_\xi} \Phi_\xi(\omega = \mathbf{0}). \tag{4.18}$$

Figures 10(a)–(c) show the values of $D_\xi(\omega)$ obtained in the β, α and molten phases, respectively, at various temperatures as a function of frequency ω. One of the common features

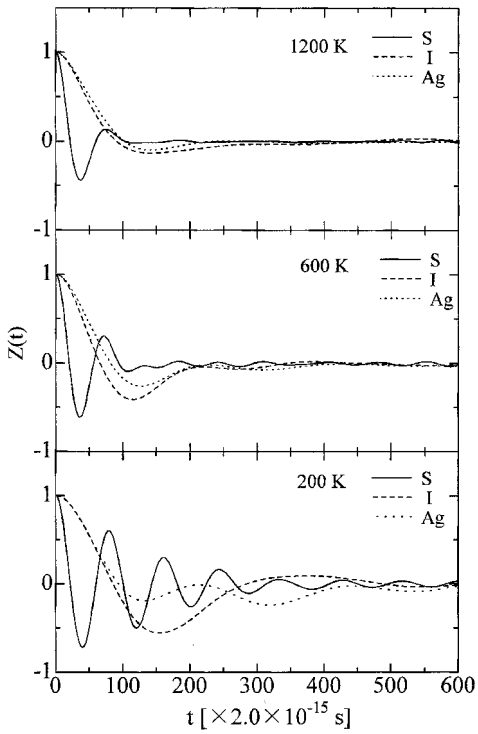

Figure 9. The VAF in the molten, α and β phases, from top to bottom, respectively.

of $D_\xi(\omega)$ is that the peaks of $D_\xi(\omega)$ become broader with increasing temperature. In the α phase, it is clearly seen that the peaks of $D_\xi(\omega)$ shift to lower frequency as the temperature increases. The static limit values of D_ξ in the molten phase and D_{Ag} in the α phase are almost the same as those obtained by the mean square displacement as reported in paper I.

As is seen in figure 10, $D_S(\omega)$ has two peaks around 10 and 37 ps^{-1} in the β phase. The first peak of $D_S(\omega)$ becomes a shoulder with increasing temperature and it cannot be seen in the molten phase. $D_I(\omega)$ has one peak at about 8–10 ps^{-1} in these three phases, which is almost the same frequency as the first peak of $D_S(\omega)$. It is interesting that the spectral density of I^- has two peaks in AgI [29], whose shape is quite different from that of Ag_3SI. In the β phase, $D_{Ag}(\omega)$ has a peak at about 4.7 ps^{-1} and a shoulder around 11 ps^{-1}. In the α phase, they become one broad peak at around 8.2 ps^{-1}, and they become a shoulder with increasing temperature in the molten phase.

As the temporal Fourier transformation of the VAF, i.e. $D_\xi(\omega)$, is proportional to the density of states of the normal modes in a harmonic system, it might be appropriate to compare $D_\xi(\omega)$ with experimental data of the density of states of the phonon [30, 31]. Shibata and Hoshino [32] performed measurements of neutron TOF spectra to obtain the generalized density of states [33] from the dynamical structure factor of Ag atoms in the β and quenched α phases of Ag_3SI. The experimental generalized density of states for Ag atoms show a resemblance to the $D_{Ag}(\omega)$ in this work, e.g., the peak positions of the generalized density of states are close to those of the $D_{Ag}(\omega)$. The experimental generalized density of states for Ag atoms has a pronounced peak at about 4.0 ps^{-1} and a shoulder around 8.4 ps^{-1} in the β phase, and a broad peak around 6.7 ps^{-1} in the quenched α phase, though we might have to take into account that the neutron TOF experimental data have a large margin of error.

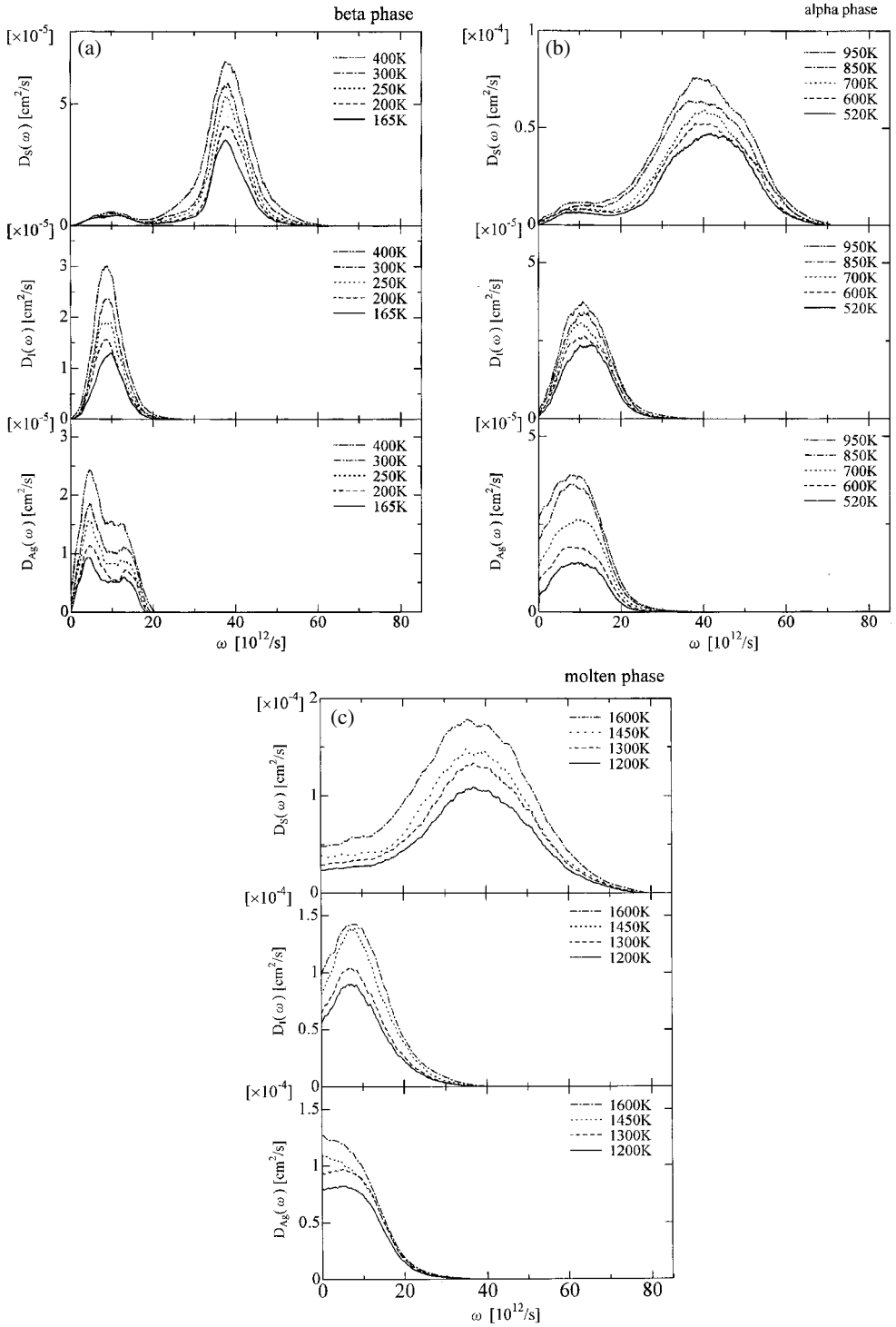

Figure 10. The frequency dependent diffusion coefficient $D_\xi(\omega)$ in the β (a), α (b) and molten (c) phases at various temperatures as a function of frequency ω.

5. Conclusions

So far, we have presented the results of the investigation of structural properties in the β phase and transport properties in the β, α and molten phases of Ag_3SI by MD. The VR-type pair potentials provide a satisfactory description of these properties of Ag_3SI. The MD results of the density distribution of Ag ions on a (1, 0, 0) plane and pair distribution functions in the β phase are in good agreement with the structures obtained by experiment.

Electric conductivities are calculated by NEMD in the α and molten phases, and by EMD in the β phase. The agreement between experiment and the simulation results is very good. The total conductivities and partial conductivities increase linearly with increasing temperature. The evaluated deviations from the Nernst–Einstein relation for cations are positive, whereas those for anions are negative. This fact may suggest that anions move collectively in the molten state. The friction constants obtained from the partial conductivities decrease as a function of temperature, which represents that the magnitude of the interference of motion decreases with increasing temperature.

In the molten, α and β phases, the amplitude of the VAF of Ag^+, S^{2-} and I^- decreases with increasing temperature. This fact may suggest that the probability of ions, which have oscillating motion, decreases with increasing temperature. The frequency dependent diffusion coefficient $D_\xi(\omega)$ is obtained from the Fourier transformation of the VAF. The static limit values of the D_ξ in the molten phase and D_{Ag} in the α phase are almost the same as the diffusion coefficients obtained by mean square displacement as we reported in paper I. The peaks of the $D_\xi(\omega)$ become broader with increasing temperature. The peaks of the $D_\xi(\omega)$ in the α phase shift to lower frequency as the temperature increases. The $D_{Ag}(\omega)$ in this work have similar features and peak positions to the generalized density of states estimated from the dynamical structure factor of Ag atoms obtained from neutron TOF spectra.

In binary ionic liquids, the relation between the ratio of the partial conductivities and masses of ions has been investigated [22]. As we have summarized above, the present result for the ionic conductivities of Ag_3SI strongly suggests that there may be another general relation between the partial conductivities in ternary ionic liquids apart from (4.8), otherwise the partial conductivities cannot converge to a certain ratio. The theoretical background of this fact will be discussed in a future work.

Acknowledgment

One of the authors (S Matsunaga) expresses his thanks to Professor S Tamaki for fruitful discussions and encouragements for this study.

References

[1] Chandra S 1981 *Superionic Solids, Principles and Applications* (Amsterdam: North-Holland)
[2] Reuter B and Hardel K 1965 *Z. Anorg. Allg. Chem.* **340** 158
[3] Reuter B and Hardel K 1965 *Z. Anorg. Allg. Chem.* **340** 168
[4] Reuter B and Hardel K 1966 *Ber. Bunsenges.* **70** 82
[5] Matsunaga S 2003 *J. Phys. Soc. Japan* **72** 1396
[6] Vashishta P and Rahman A 1978 *Phys. Rev. Lett.* **40** 1337
[7] Vashishta P, Ebbsjo I, Dejus R and Skold K 1985 *J. Phys. C: Solid State Phys.* **18** L291
[8] Hull S, Keen D A, Gardner N J G and Hayes W 2001 *J. Phys.: Condens. Matter* **13** 2295
[9] Ihara S and Suzuki K 1985 *J. Phys. Soc. Japan* **54** 2607
[10] Kobayashi M, Shimojo F, Tachibana F and Okazaki H 1991 *J. Phys. Soc. Japan* **60** 245
[11] Didisheim J-J, McMullan R K and Wuensch B J 1986 *Solid State Ion.* **18/19** 1150
[12] Nose S 1984 *J. Chem. Phys.* **81** 511

[13] Verlet L 1967 *Phys. Rev.* **159** 98
[14] Hoshino S, Sakuma T and Fujii Y 1978 *J. Phys. Soc. Japan* **45** 705
Hoshino S, Sakuma T and Fujii Y 1979 *J. Phys. Soc. Japan* **47** 1252
[15] Perenthaler E and Schulz H 1981 *Solid State Ion.* **2** 43
[16] Cho N, Kikkawa S, Kanamaru F and Yoshiasa A 1994 *Solid State Ion.* **68** 57
[17] Hansen J-P and McDonald I R 1986 *Theory of Simple Liquids* 2nd edn (London: Academic)
[18] Matsunaga S 2001 *J. Phys. Soc. Japan* **70** 3591
[19] Matsunaga S 2002 *J. Non-Cryst. Solids* **312** 409
[20] Tubandt C and Lorenz E 1914 *Z. Phys. Chem.* **87** 513
Tubandt C and Lorenz E 1914 *Z. Phys. Chem.* **87** 543
[21] Ohno S, Ishida K, Togashi M and Okada T 2000 *J. Phys. Soc. Japan* **69** 1443
[22] Koishi T, Arai Y, Shirakawa Y and Tamaki S 1997 *J. Phys. Soc. Japan* **66** 3188
[23] Koishi T, Kawase S, Tamaki S and Ebisuzaki T 2000 *J. Phys. Soc. Japan* **69** 3291
[24] Chiodelli G, Magistris A and Schiraldi A 1979 *Z. Phys. Chem.* **118** 177
[25] Yokota I 1966 *J. Phys. Soc. Japan* **21** 420
[26] Koishi T and Tamaki S 1999 *J. Non-Cryst. Solids* **250–252** 501
[27] Koishi T and Tamaki S 1999 *J. Phys. Soc. Japan* **68** 964
[28] Rahman A and Vashishta P 1983 *Physics of Superionic Conductors* ed J W Perrum (New York: Plenum)
[29] O'Sullivan K, Chiarotti G and Madden P A 1991 *Phys. Rev.* B **43** 536
[30] Balucani U and Zoppi M 1994 *Dynamics of the Liquid State* (Oxford: Clarendon)
[31] Bruesch P 1982 *Phonons: Theory and Experiments I* (*Springer Series on Solid-State Sciences* vol 34) (Berlin: Springer)
[32] Shibata K and Hoshino S 1985 *J. Phys. Soc. Japan* **54** 3671
[33] Lomer W M and Low G G 1965 *Thermal Neutron Scattering* (New York: Academic)